THE ASTROPHYSICAL JOURNAL, 303:L45–L49, 1986 April 15

NGC 4261: A PROLATE ELLIPTICAL GALAXY

ROGER L. DAVIES
Kitt Peak National Observatory, National Optical Astronomy Observatories
AND
M. BIRKINSHAW[1]
Department of Astronomy, Harvard University
Received 1985 October 25; accepted 1986 January 21

ABSTRACT

Long-slit spectra for the E2 galaxy NGC 4261 show that its projected rotation axis lies only $6° \pm 4°$ from its projected major axis. This observation suggests that the intrinsic figure of the galaxy is prolate: if the galaxy is oblate, then its rotation axis is almost perpendicular to its symmetry axis. The angular momentum vector of the stars may be parallel to either the shortest or the longest axis of the galaxy, so that NGC 4261 may be either a bar or a spindle.

Subject headings: galaxies: individual — galaxies: internal motions — galaxies: structure

I. INTRODUCTION

The intrinsic figures of elliptical galaxies are of interest in establishing the range of forms that arise as endpoints of galaxy formation and in the interpretation of kinematical data. Statistical tests intended to distinguish between oblate and prolate figures, by investigating the dependence of surface brightness or velocity dispersion on observed axial ratio (Marchant and Olson 1979; Richstone 1979; Lake 1979; Olson and de Vaucouleurs 1981), have not reached a consistent conclusion. It is known that elliptical galaxies are not oblate spheroids flattened by rotation, because their rotation velocities are too low (Bertola and Capaccioli 1975; Illingworth 1977), but if elliptical galaxies are supported by anisotropic pressure, oblate, prolate, or triaxial figures are possible (Binney 1978).

To date, no convincing case of a prolate galaxy has been identified. The most nearly prolate case so far described is that of NGC 596 (Williams 1981): this galaxy, which displays a 60° isophote twist, rotates about an axis that changes with radius and is nowhere coincident with the projected minor axis. In its outer parts NGC 596 rotates about its long axis and is prolate.

In this *Letter* we present our observations of NGC 4261, a morphologically simple E2 galaxy, and demonstrate that its rotation axis lies close to its projected major axis at all radii. NGC 4261 resides in the Virgo W cloud (de Vaucouleurs 1975), a group with high velocity compared to the Virgo Cluster (the heliocentric velocity is 2237 km s^{-1}). We assume that NGC 4261 is a member of the Virgo Cluster, which we take to be at a distance of 20 Mpc, so that $M_B = -22.1$.

[1]Visiting Astronomer at Kitt Peak National Observatory, NOAO, operated by the Association of Universities for Research in Astronomy, Inc., under contract with the National Science Foundation.

II. THE DATA AND ANALYSIS

Long-slit spectra of NGC 4261 were taken at four position angles using the Cryogenic Camera on the KPNO 4 m telescope on 1984 February 26. The Cryogenic Camera is described in De Veny (1983), and was used with a 2″.5 slit and the 400 lines mm^{-1} grism (number 650), giving spectra from 4150 to 6350 Å with resolution (FWHM) ≈ 11 Å. The slit was 4′.5 in length, and one pixel on the detector corresponded to 3 Å × 0″.86. Integrations of 30 minutes duration were taken with the galaxy centered on the slit at PA 11°, 71° (near the minor axis), 131°, and 161° (near the major axis). The seeing during the observations was typically 2″.5. A sky spectrum and spectra of nine G and K giants were taken during the twilight hours of the run. Calibration spectra of quartz and He-Ne-Ar lamps were taken at each slit position.

All spectra were bias-subtracted, and the quartz lamp spectra were flattened, normalized, and divided into the data to remove sensitivity variations over the CCD detector. The sky spectrum was used to generate a correction for vignetting. Geometric distortions of the spectra were mapped using lines in the He-Ne-Ar lamp spectra: the rms residual was typically 10 km s^{-1} per line. The data were rebinned into equal logarithmic wavelength intervals of 220 km s^{-1}. The small distortion in the spatial direction was removed by tracing the galaxy center and rebinning. These reduction procedures have been discussed and tested elsewhere (e.g., Kormendy and Illingworth 1982).

A region of 512 pixels (extending from 4210 to 6130 Å) by 280 pixels was extracted from the data. A sky spectrum was generated by averaging 20 rows close to the ends of each spectrum, and this was then subtracted from the data. Variations in focus across the detector cause the strong 5461, 5577, and 5893 Å sky lines to subtract poorly, and they were interpolated over in the Fourier analysis.

The calibrated, sky-subtracted spectra were analyzed using the Fourier Quotient method due to Schechter (Sargent *et al.*

1977; Kormendy and Illingworth 1982). Tests were carried out to find the best-fitting star spectrum: the K1 III star HD 134585 was chosen, and fits of the quotient of the Fourier transforms of the galaxy and the star spectra used wavenumbers $k = 12$ to 128.

III. RESULTS

The folded velocity measurements are shown in Figure 1. Typically these extend to radii of 50″ with uncertainties of ± 20 km s^{-1} at the center of the galaxy and ± 50 km s^{-1} at larger radii. No rotation is observed in the central 5″, but beyond that rotation is detected in PAs 11°, 71°, and 131°, in the sense that the NE of the galaxy is receding. A maximum amplitude of about 100 km s^{-1} is measured in PA 71°.

These velocity measurements imply that NGC 4261 is rotating about an axis close to PA 161°. We reproduce as Figure 2 the major axis PA and ellipticity of NGC 4261 as functions of radius measured by Peletier *et al.* (1986); together these results show that NGC 4261 is rotating about an axis close to its projected major axis over the entire range of radii covered by the data. In view of the surprising nature of this result, we carried out a thorough check of the calibration and analysis. The peak-to-peak rotation at PA 71° is far larger than the uncertainties in the wavelength calibration. When the position of the 5461 Å sky line was traced in the geometrically-calibrated spectra, it was found to shift blueward by 20 km s^{-1} from radii 45″ east to 45″ west of the nucleus at all PAs. This shift is insufficient to account for the observed rotation and it results from a change in character of the line profile due to the changing focus across the detector. We find no evidence for any systematic effect which could either cancel or mimic a rotation as large as 100 km s^{-1}. We can also eliminate the possibility that the major and minor axes were confused. Figure 3 (Plate L5) shows a bright object about 70″ from the center of NGC 4261 in PA 71°. This object appears prominently on the spectrum for which we measure a rotation velocity of 100 km s^{-1}. Thus there can be no doubt that NGC 4261 exhibits substantial rotation on its minor axis.

We have measured the velocity dispersion profile at each position angle, and these results will be reported fully in a later paper (Davies and Birkinshaw 1986). We find a central velocity dispersion ≈ 320 km s^{-1} (in good agreement with Schechter 1980 and Tonry and Davis 1981), falling to ≈ 280 km s^{-1} at a radius of 30″. There are no significant differences between the dispersion profiles at the four position angles.

In Figure 1, the uncertainties on each point appear to be overestimated compared to the scatter of measurements from opposite sides of the center. Davies and Illingworth (1983) noted that the errors on similar measurements of NGC 3379 were too large by a factor of 1.5 compared to the scatter in independent measurements. For the purpose of comparison with models (§ IV), the errors have been reduced by a factor of 1.5.

A previous measurement of the rotation of NGC 4261 was made by Jenkins (1981). At PA 90°, Jenkins found a rotation

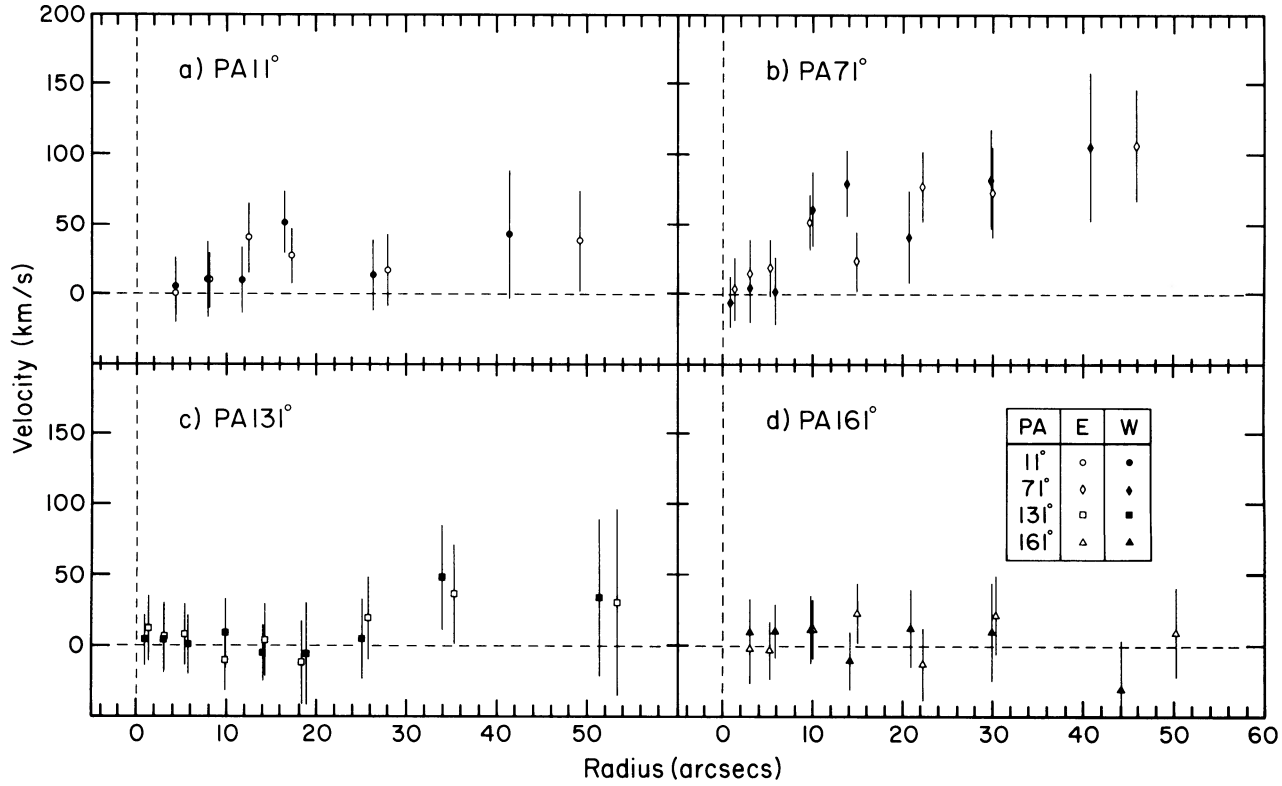

FIG. 1.—The measured velocities as a function of radius for each of the four slit positions. The velocity measurements have been folded about the center of the galaxy, with velocities to the west changed in sign for all slits except that at PA 161°, where the velocities to the east were flipped.

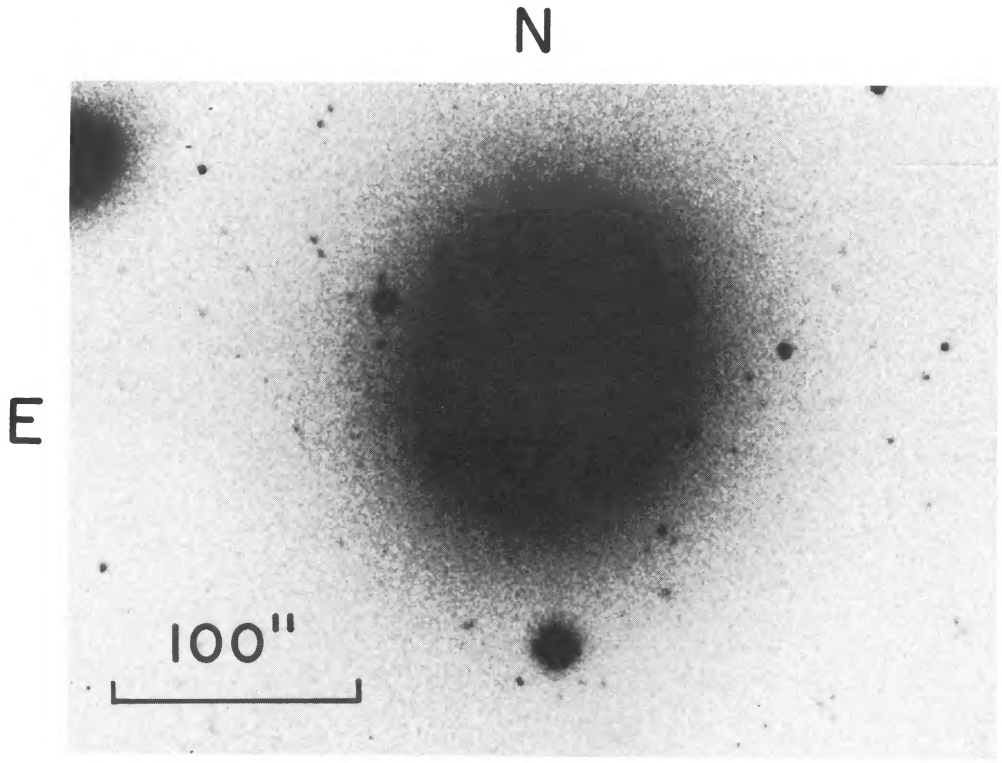

FIG. 3.—NGC 4261 from an *R* band CCD frame. The object lying about 70″ in PA 71° from the center of NGC 4261 appears on the PA 71° slit and confirms that this slit shows the greatest rotation velocity. NGC 4264 appears to the far NE of this frame.

DAVIES AND BIRKINSHAW (*see* page L46)

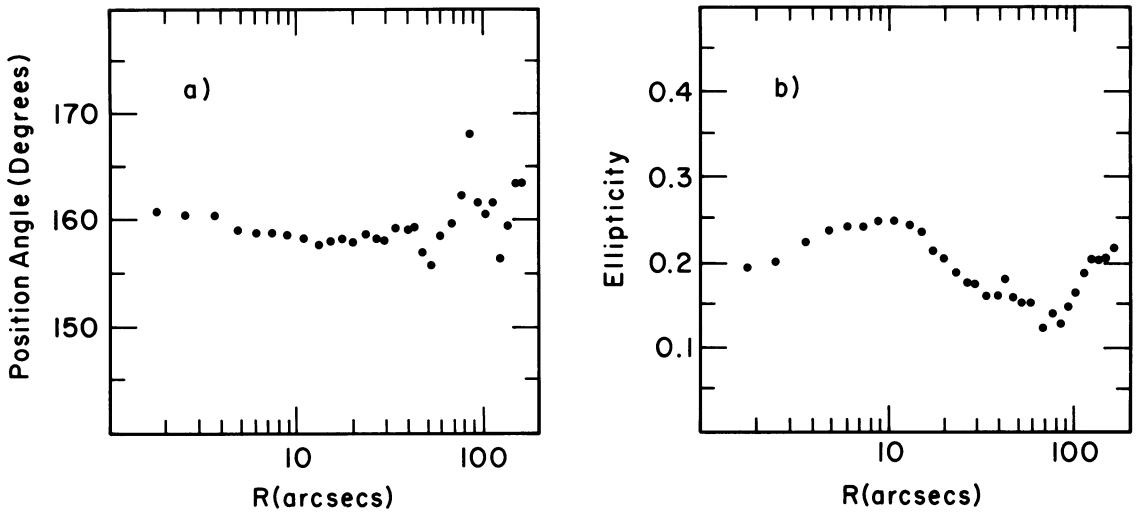

FIG. 2.—The ellipticity and major axis position angles for NGC 4261 as functions of radius R, reproduced from Peletier *et al.* (1986)

of 350 km s^{-1} at radius 40″, in the sense that the east side of the galaxy is approaching relative to the center. At PA 180°, Jenkins found a rotation in the sense that the south side of the galaxy recedes at 40 km s^{-1} for radii less than 12″, with no rotation at larger radii. He quotes a value of 440 km s^{-1} for the mean velocity dispersion at radii less than 20″. Our data in four PAs are inconsistent with such a velocity field.

The data of Figure 2 show that NGC 4261 is a normal galaxy by comparison with NGC 596 (Williams 1981). NGC 4261 shows less than $\approx 4°$ of isophotal twist, and its ellipticity remains near 0.17 over a wide range of radii. Our spectra show no emission lines from the nucleus of NGC 4261 —the limit on the equivalent width of the 5007 Å line is 1 Å for a feature 800 km s^{-1} wide. Inspection of a $B - R$ color map formed from the data of Peletier *et al.* (1986) shows no obvious evidence of dust. Thus NGC 4261 appears to be a well-defined prolate galaxy, without complicating features.

IV. DISCUSSION

The PA of the projected rotation axis of NGC 4261 can best be measured by modeling the velocity field of the galaxy. This has been done using the phenomenological model described by Davies and Birkinshaw (1986), which is similar to the kinematical model of Binney (1985): the model luminosity density is the same triaxial function with semi-axes (a, b, c), and the rotation law is of the form $\omega(u) \propto (d^2 + u^2)^{-1/2}$, where u is either the distance from the galaxy center ("spherical"), or the distance from the axis of rotation ("cylindrical"). The parameter d sets the length scale of the velocity law. Additional parameters are used to describe the orientation of the rotation axis in the frame of the galaxy (inclination and azimuthal angles θ, ϕ), and the projection transformation between the coordinate frames of the galaxy and the observer (Euler angles α, β, γ). Note that we do not assume that the rotation axis is coincident with a principal axis of the galaxy.

The results (Fig. 2) that the PA of the major axis of the projected figure $\Gamma_{maj} \approx 159°$ and the ellipticity of the projected figure $\varepsilon \approx 0.17$, and the requirement that the true figure of the galaxy be rounder than E6, constrain the axial ratios b/a, c/a and the Euler angles (α, β, γ) to occupy a three-dimensional subspace of the full five-dimensional parameter space. The scale of the galaxy is set by the core radius, a, taken as 2.″6, the seeing-deconvolved result of Lauer (1985).

With these data and constraints, all but two of the angular parameters may be fitted. These angles may conveniently be taken as α (one of the Euler angles) and ϕ (the azimuthal angle of the rotation axis in the frame of the galaxy). In practice, the choice of (α, ϕ) does not affect strongly the fitted values of the important kinematical parameters (Γ_r, the PA of the projected rotation axis; v_{max}, the peak projected rotation velocity of the galaxy; and d/a, the ratio of the rotation and luminosity length scales). The radial sampling and the effects of seeing were taken into account in calculating the intensity-weighted radial velocity function that is fitted. Since the slits overlap near the galaxy center, the number of independent data points is less than the number of sample points. This effect is approximately constant from model to model, so that the effective number of degrees of freedom of χ^2 is about 47, 10 less than the apparent number in each model.

Several possibilities for the intrinsic figure of NGC 4261, spanning prolate, oblate, and triaxial structures, were tested using this model. Fits with both spherical and cylindrical rotation laws were performed; we found that spherical models are marginally superior. The results of representative fits of this type are shown in Table 1. We find $\Gamma_r = 333° \pm 4°$ to be a good estimate for the position angle of the projected angular momentum vector (almost independent of the choice of model), $d/a = 11 \pm 5$ (poorly constrained by the data, since the rotation curves show no convincing turn-over), and $v_{max} = 101 \pm 22$ km s^{-1}. The values of d/a and v_{max} are strongly correlated, so that the large uncertainty in d/a produces a large error in v_{max}.

These results confirm, quantitatively, the conclusion of § III that the projected major and rotation axes of NGC 4261 are parallel. The projected major axis lies in PA $\Gamma_{maj} = 159° \pm 2°$ (Peletier *et al.* 1986), so that $(\Gamma_{maj} - \Gamma_r) = 6° \pm 4°$. Thus we conclude that NGC 4261 is prolate, or triaxial and close to

TABLE 1

MODEL FITS TO NGC 4261

Model Type	$\frac{b}{a}$	$\frac{c}{a}$	$\frac{d}{a}$	$\Gamma_{maj} - \Gamma_r$ (degrees)	v_{max} (km s^{-1})	χ^2 (47 d.o.f.)
PS.....	0.80	0.80	10.4 ± 2.5	7 ± 2	100 ± 22	49.2
	0.50	0.50	10.9 ± 3.7	7 ± 3	102 ± 12	47.9
PB.....	0.80	0.80	10.4 ± 4.6	6 ± 4	102 ± 20	49.2
	0.50	0.50	10.4 ± 5.4	7 ± 4	98 ± 19	47.9
O	1.00	0.80	12.0 ± 4.2	6 ± 2	112 ± 19	49.4
	1.00	0.50	12.3 ± 5.7	5 ± 3	98 ± 25	49.9
T.....	0.85	0.70	11.9 ± 7.3	6 ± 4	99 ± 28	49.2
	0.75	0.50	9.6 ± 3.2	7 ± 3	85 ± 12	48.6
R.....	0.83	0.77	9.5 ± 3.5	6 ± 3	111 ± 22	49.3
	0.86	0.69	8.5 ± 3.7	7 ± 3	107 ± 25	49.6

NOTES.—(1) The models have spherical rotation laws and are oblate (O), prolate (P), triaxial (T), or triaxial subject to the radio constraint (R). Both spindle (S) and bar (B) prolate models have been constructed. A free fit of the rotation axis was performed for all but the PB models. Oblate models rotate about axes almost perpendicular to their symmetry axes, and are implausible representations of NGC 4261. (2) The error estimates for d/a, Γ_r, and v_{max} include a contribution from the indeterminacy of angles α and ϕ. Γ_{maj} has been taken as 159°.

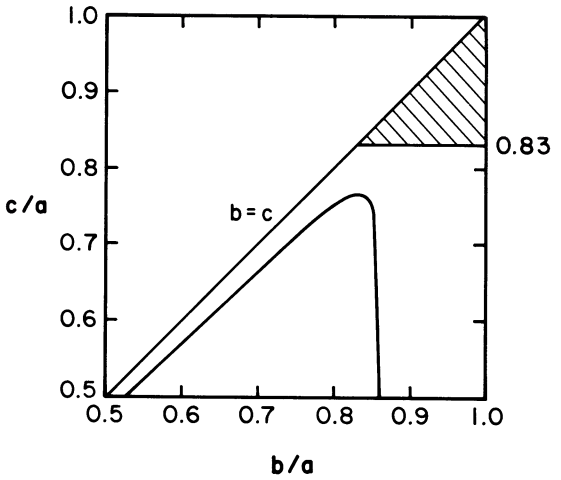

FIG. 4.—The permitted values of b/a and c/a under the assumption that the radio axis of NGC 4261 is the shortest principal axis. No true oblate or prolate model is acceptable, since the minor and radio axes are misaligned. The shaded region is excluded by the constraint of the observed ellipticity of the galaxy.

prolate. Oblate models can be fitted to NGC 4261, but such models require the unlikely condition that the rotation axis lies almost perpendicular to the symmetry axis of the spheroid.

Since the projected rotation axis and projected longest axis of NGC 4261 are almost parallel, the galaxy is being viewed so that its rotation and longest axes and the line of sight are nearly coplanar. We consider two specific prolate configurations, the first with the longest and rotation axes coincident (the spindle case), and the second with the longest and rotation axes perpendicular (the bar case). In the spindle case, the rotation and longest axes are always coplanar with the line of sight. Binney (1985) has shown that for this configuration the radial velocity on the projected minor axis is much larger than that on the projected major axis for almost all viewing angles, as is the case for this galaxy.

For the bar case, the rotation and longest axes of NGC 4261 lie near a common plane with the line of sight for only a small range of viewing orientations. If the galaxy is triaxial, but close to prolate, the range of viewing angles that produce small projected velocities on the major axis is further reduced. A bar configuration is allowed by the data, but imposes severe limitations on the possible viewing angles. We cannot use this restricted range of viewing angles to conclude that a bar configuration is unlikely because it was the coincidence of Γ_{maj} and Γ_r that brought NGC 4261 to our attention.

One further piece of configurational information on NGC 4261 is available through the radio structure of the galaxy (Birkinshaw and Davies 1985). If we assume that the long, straight radio jets (in PA 88°) lie close to a principal axis of the galaxy, then the allowed combinations of axial ratio are reduced to those in Figure 4. Under this hypothesis, the c-axis is the radio axis and NGC 4261 is triaxial, with

$$0.86 \geq \frac{b}{a} \geq 0.52 \qquad 0.77 \geq \frac{c}{a} \geq 0.50,$$

and the minimum possible ellipticity arises at $(b/a, c/a) = (0.83, 0.77)$. The two R-models in Table 1 satisfy this radio constraint and lead to similar values for v_{max} and Γ_r as the other models in the table, but are of particular interest because of their capacity for incorporating the radio data into a consistent model for NGC 4261.

V. CONCLUSIONS

1. The projected rotation axis of the morphologically simple elliptical galaxy NGC 4261 lies only 6° ± 4° from its projected major axis.

2. We suggest that the figure of NGC 4261 is prolate (or triaxial but close to prolate). Both "bar" (rotation and longest axes perpendicular), and "spindle" (rotation and longest axes parallel) configurations are allowed. The bar configuration requires a more restrictive viewing geometry.

3. If we assume that the radio jets escape along the shortest axis of the galaxy, then the figure of the NGC 4261 is triaxial with $0.86 \geq b/a \geq 0.52$ and $0.77 \geq c/a \geq 0.50$.

4. Prolate or near-prolate figures can be generated in the process of galaxy formation. Since low-luminosity elliptical galaxies and the bulges of spiral galaxies are almost certainly close to oblate (Davies *et al.* 1983; Kormendy and Illingworth 1982), the full range of ellipsoidal figures is realised among early-type galaxies. Thus any analysis that assumes a universal figure for these galaxies (e.g., in the inversion of the projected distribution of axial ratios to the true distribution of galaxy figures, or the study of the three-dimensional orientations of radio jets by comparison of the apparent jet and minor axes) will require revision.

We are grateful to Garth Illingworth for helpful discussions on the kinematics of NGC 4261.

REFERENCES

Bertola, F., and Capaccioli, M. 1975. *Ap. J.*, **200**, 439.
Binney, J. 1978. *M.N.R.A.S.*, **183**, 501.
_____. 1985. *M.N.R.A.S.*, **212**, 767.
Birkinshaw, M., and Davies, R. L. 1985. *Ap. J.*, **291**, 32.
Davies, R. L., and Birkinshaw, M. 1986, in preparation.
Davies, R. L., Efstathiou, G., Fall, S. M., Illingworth, G., and Schechter, P. L. 1983, *Ap. J.*, **266**, 41.
Davies, R. L., and Illingworth, G. 1983. *Ap. J.*, **266**, 516.
de Vaucouleurs, G. 1975, in *Stars and Stellar Systems*, Vol. **9**, *Galaxies and the Universe*, ed. A. Sandage, M. Sandage, and J. Kristian (Chicago: University of Chicago Press), p. 556.
De Veny, J. 1983, *An Observers' Manual for the Cryogenic Camera*, Kitt Peak National Observatory.
Illingworth, G. 1977, *Ap. J.* (*Letters*), **218**, L43.
Jenkins, C. R. 1981, *M.N.R.A.S.*, **196**, 987.
Kormendy, J. and Illingworth, G. 1982. *Ap. J.*, **256**, 460.
Lake, G. 1979, in *Photometry, Kinematics, and Dynamics of Galaxies*, ed. D. S. Evans (Austin: University of Texas Press), p. 381.
Lauer, T. 1985, *Ap. J.*, **292**, 104.
Marchant, A. B., and Olson, D. W. 1979, *Ap. J.* (*Letters*), **230**, L157.
Olson, D. W. and de Vaucouleurs, G. 1981. *Ap. J.*, **249**, 68.
Peletier, R., Davies, R. L., Illingworth, G. D. Davis, L. and Cawson, M. 1986, in preparation.
Richstone, D. 1979, *Ap. J.*, **234**, 825.
Sargent, W. L. W., Schechter, P. L., Boksenberg, A., and Shortridge, K. 1977, *Ap. J.*, **212**, 326.
Schechter, P. L. 1980, *A.J.*, **85**, 801.
Tonry, J. L., and Davis, M. 1981. *Ap. J.*, **246**, 666.
Williams, T. B. 1981, *Ap. J.*, **244**, 458.

M. BIRKINSHAW: Department of Astronomy, Harvard University, 60 Garden Street, Cambridge, MA 02138

R. L. DAVIES: Kitt Peak National Observatory, National Optical Astronomy Observatories, 950 North Cherry Avenue, P.O. Box 26732, Tucson, AZ 85726-6732

PLATE L6

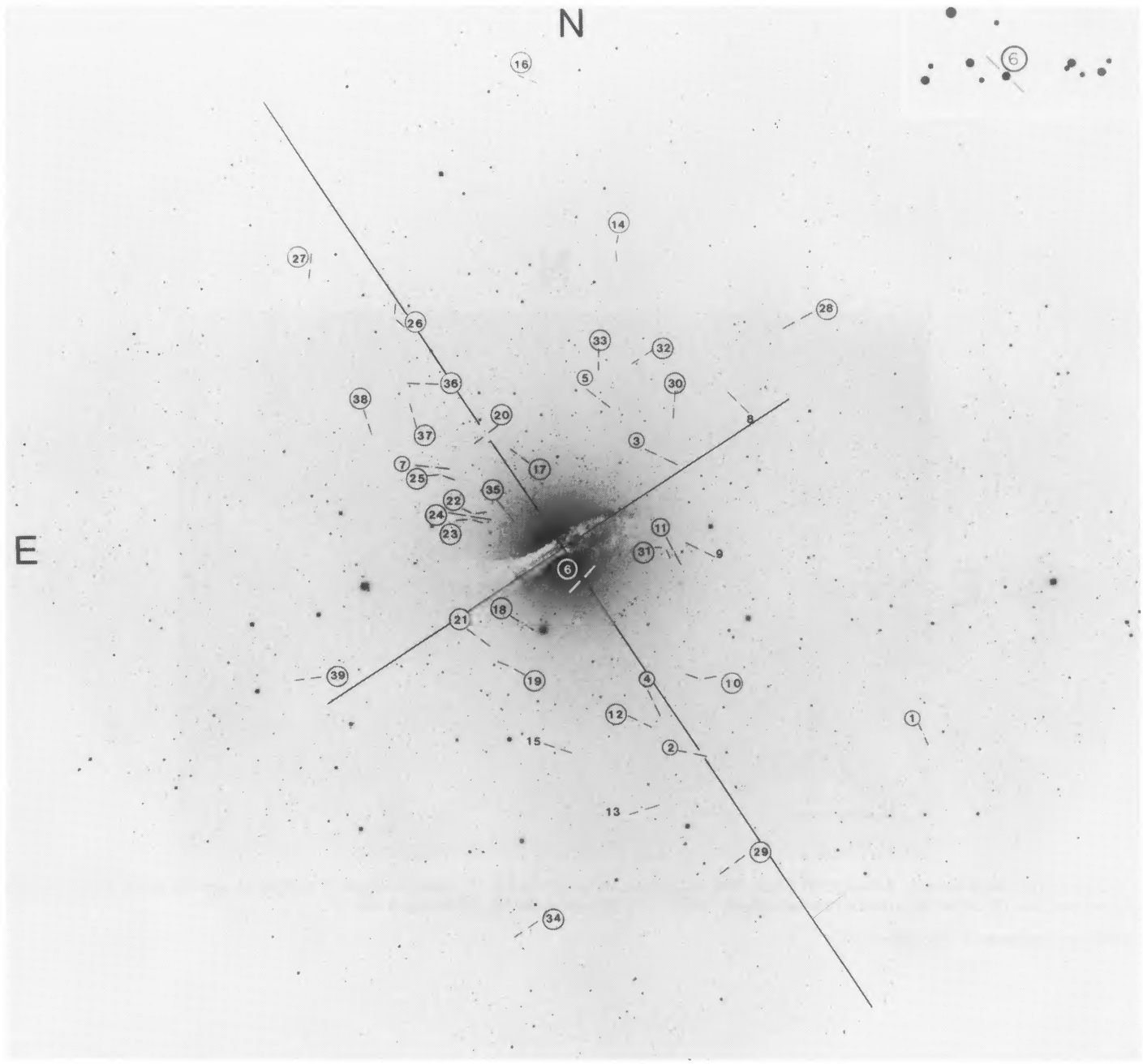

FIG. 1.—Identification of spectroscopically confirmed clusters (*circled numbers*) and cluster candidates (*uncircled*—see Paper II). The axes adopted for measurement of orthogonal distances are shown, where that running NE–SW (roughly parallel to the radio axis) is assumed to be the major axis.

HESSER, HARRIS, AND HARRIS (*see* page L52)